PROCEEDINGS OF SCIENCE

Towards a 3D Neutrino Tomography of the Earth's mantle

Rebekah Pestes,[a,b] **João A. B. Coelho,**[a] **Stéphanie Durand,**[c] **Nobuaki Fuji,**[b,d] **Edouard Kaminski,**[b] **Lukas Maderer**[a] **and Véronique Van Elewyck**[a,d,*]

[a] *Astroparticule et Cosmologie, CNRS, Université Paris Cité, Paris, France*

[b] *Université Paris Cité, Paris, Institut de physique du globe de Paris, CNRS, France*

[c] *Laboratoire de Géologie de Lyon : Terre, Planètes, Environnement, CNRS, UMR 5276, École Normale Supérieure de Lyon, Université de Lyon, Université Claude Bernard Lyon 1*

[d] *Institut Universitaire de France, Paris, France*

E-mail: rpestes@apc.in2p3.fr, nobuaki@ipgp.fr, elewyck@apc.in2p3.fr

Neutrinos can be used to study the interiors of various objects that are difficult to fully probe by classical means. In the case of the Earth, neutrinos provide complementary information to seismic waves because of the imprint of matter effects on their oscillations. This alternative approach may bring new insights on open questions regarding the composition, structure and dynamics of the deep Earth, for example concerning the nature and origin of the large-scale inhomogeneities observed in the lower mantle and known as large low-shear velocity provinces (LLSVPs). In order to be able to explore the potential of present- and future-generation atmospheric neutrino detectors for probing asymmetric models of the Earth's mantle, we extended the capabilities of the OscProb programming library to handle calculating oscillation probabilities for a neutrino trajectory defined by both the zenith and azimuthal angles through an Earth model binned in 3 dimensions: depth, latitude, and longitude. An example using a simplistic model of an LLSVP is provided to demonstrate how this new version of OscProb can be used.

38th International Cosmic Ray Conference (ICRC2023)
26 July - 3 August, 2023
Nagoya, Japan

*Speaker

PoS(ICRC2023)1162

1. Introduction

One of the most powerful tools for imaging the present-day structure of the Earth's interior are seismic waves. They are generated by earthquakes and propagate inside the Earth, probing every layer of it. Their travel times and amplitudes reveal information about the elastic, anelastic and density structure of the Earth. Since the first record of a teleseismic event (Tokyo-Potsdam) in 1889 [1], modern seismology has made tremendous progresses in revealing the 1D and 3D features of the Earth's interior. The averaged depth dependency of the Earth's physical properties, such as density and elasticity, is known to within a few percent [2], and since the 90's, lateral heterogeneity with respect to PREM has been mapped with improving resolution thanks to the increase in the amount of data as well as in computational power. One of the very first large-scale heterogeneities revealed by the 3D seismic imaging of the Earth's mantle are the two large low-shear-velocity provinces (or LLSVPs) that sit at the base of the mantle beneath the Pacific and Africa [3]. They are seen as more or less heterogeneous dome-like structures [4, 5] at which mantle plumes might be anchored [6]. LLSVPs are therefore believed to play a critical role in mantle dynamics and Earth's evolution. For instance, they could be a residual of the crystallization of a basal magma ocean [7] or a collection of primordial material brought to the base of the mantle in an early stage of the Earth. Also important is the question of LLSVPs stability in time. Different scenarios could be better disentangled if the nature of these LLSVPs - purely thermal or thermo-chemical - were known [8, 9].

A renewed perspective on these questions may come from atmospheric neutrino oscillation tomography, an approach which provides direct sensitivity to the electron density along the neutrino path (see e.g. [10–12] and references therein). Cosmic rays interacting with the Earth's atmosphere generate an almost isotropic flux of neutrinos, most of which are able to traverse the Earth without being absorbed nor deflected. Flavour oscillations of such neutrinos are modified with respect to vacuum oscillations due to coherent forward scattering on electrons along their propagation path. An accurate measurement of this effect, based on the angular, energy and flavour distribution of neutrinos interactions observed in detectors at the surface of the Earth, can therefore provide sensitivity to the electron density N_e in the different layers of matter traversed.

The ratio of electron density (N_e) to mass density (ρ_m) scales with the average proton to nucleon ratio (denoted Z/A), which depends on the chemical and isotopic composition of the medium:

$$N_e = (N_A/m_n)(Z/A)\rho_m,$$

where N_A is the Avogadro number and m_n the nucleon mass. With the Z/A ratio being equal to 1 for hydrogen, constraining N_e can be useful to infer information on the distribution of volatile elements in the inner Earth, whose budget is hard to estimate from seismic data alone because it is challenging to constrain experimentally due to the extreme conditions. Obtaining a 1D/3D N_e distribution inside the Earth, even with low resolution, could therefore help constrain the thermo-chemical evolutionary history of the solid Earth.

2. Simulations with OscProb

OscProb [13] is a C++ programming library, compatible with ROOT [14], that calculates oscillation probabilities for neutrinos traveling through matter, breaking their trajectories into pieces

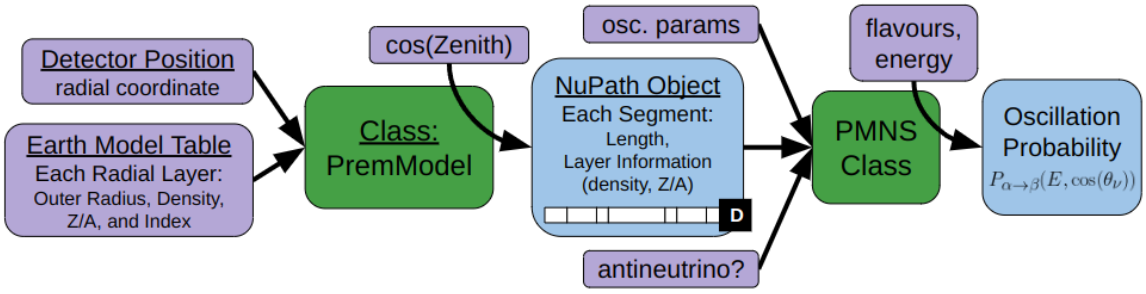

Figure 1: Diagram of the standard workflow for using OscProb. The main classes used are shown in green, the inputs are shown in purple, and the outputs are shown in blue.

with a constant matter profile. A flowchart describing the baseline implementation of the library is presented in figure 1, with the corresponding geometrical setup illustrated in the left panel of figure 2. It relies on a class, called PremModel, which assumes that the Earth is spherically symmetric for the purposes of calculating neutrino trajectories. PremModel takes as inputs the detector position as defined by its radial coordinate r_d, and a table containing the matter profile for each layer of the Earth, binned in radius. As a default Earth model, it uses a density profile based on the Preliminary Reference Earth Model (PREM) [2] with geochemical reservoirs approximated from data in the Geochemical Earth Reference Model (GERM) [15].

The FillPath function within PremModel calculates a neutrino's trajectory, given the cosine of its zenith angle θ_ν (as measured from the upward vertical at the detector location), with the neutrino position along its path being measured by its distance d_x from the detector position. It starts at the location where the neutrino enters the Earth and loops over the radius bins crossed along the way to the detector, to find the distance traveled in each bin. The collection of segments, each characterized by a length, density and Z/A values, making up the neutrino trajectory is stored as a NuPath object that can then be fed into one of the PMNS classes in order to calculate oscillation probabilities along the neutrino path. While different oscillation models are available in OscProb, including e.g. sterile neutrinos, non-standard interactions or neutrino decay, in this work we used exclusively the PMNS class with standard 3-neutrino oscillations.

3. Implementation of a 3D Earth Model

In order to allow for lateral inhomogeneities inside the Earth, we augmented OscProb with the ability to accept a matter profile that is split up into latitude and longitude bins, in addition to radial bins, and a detector position specified with its latitude θ_d and longitude ϕ_d, in addition to its radial coordinate r_d. This was done through the creation of a new class, called EarthModelBinned. In order to keep from duplicating code between PremModel and EarthModelBinned, we also created a base class, called EarthModelBase, from which PremModel and EarthModelBinned are derived.

In the EarthModelBinned class, we revamped the FillPath function to fully accommodate the use of a 3D matter profile. The corresponding, 3D geometrical setup is shown in the right panel of figure 2. While in PremModel, only the zenith angle θ_ν was needed as an argument of FillPath in order to calculate the neutrino's trajectory, in the more general setup of EarthModelBinned, we

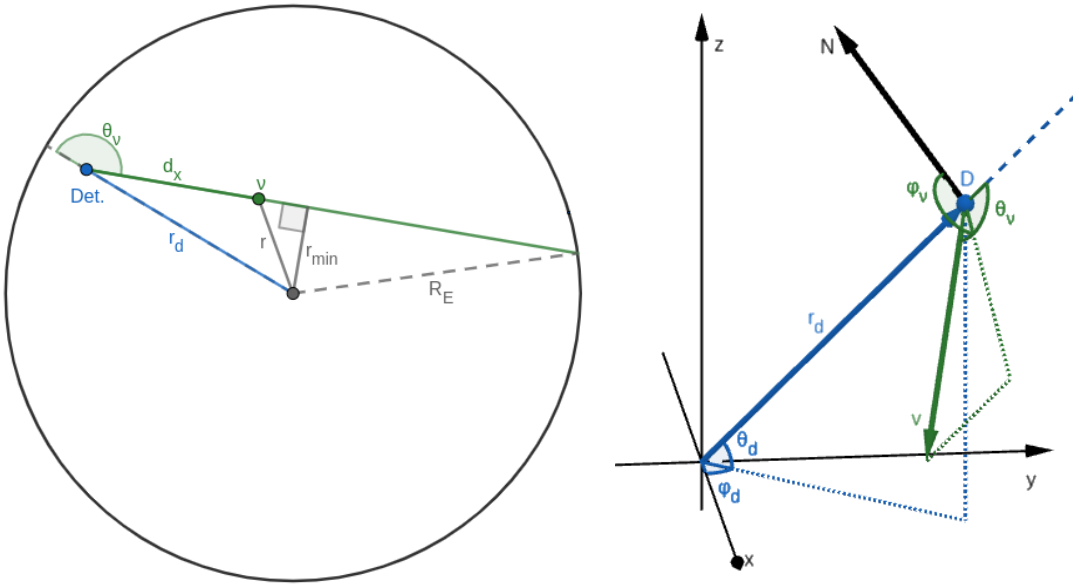

Figure 2: Diagram of a neutrino's trajectory (green) with the detector location (blue) shown in two views: 1) on the left, in a plane through the Earth containing the Earth's center, the detector, and the point at which the neutrino entered the Earth and 2) on the right, as a vector in 3D space.

added the azimuthal angle ϕ_ν (specified as degrees counter-clockwise from North) of the neutrino's trajectory to FillPath's arguments. Based on these inputs, FillPath now finds the latitude and longitude where the neutrino with this trajectory enters the Earth. Starting from this entry point, it loops over the depth bins crossed by the neutrino's trajectory, but now checking for latitude and longitude bin crossings before recording the trajectory segment remaining until the next depth bin.

For an incident neutrino with zenith angle θ_ν and azimuthal angle ϕ_ν reaching a detector at coordinates $(r_d,\ \theta_d,\ \phi_d)$, one can define the unit vector pointing from the detector towards the neutrino's source as:

$$\hat{v} = \cos\theta_\nu \hat{r}_d + \sin\theta_\nu \left[\cos\phi_\nu \hat{\theta}_d - \sin\phi_\nu \hat{\phi}_d\right] , \tag{1}$$

where $\hat{r}_d$ is a unit vector pointing to the detector from the center of the Earth, $\hat{\theta}_d$ is a unit vector pointing north from the detector, and $\hat{\phi}_d$ is a unit vector pointing east from the detector. Using this definition, the vector pointing from the center of the Earth to a point on the trajectory a distance d_x away from the detector is $\vec{x}_\nu = d_x\hat{v} + \vec{r}_d$. The coordinates (in radius r, latitude θ, and longitude ϕ) for this point can then be expressed as:

$$r(d_x) = \|\vec{x}_\nu\| , \quad \sin\theta(d_x) = \frac{\vec{x}_\nu \cdot \hat{z}}{\|\vec{x}_\nu\|} , \quad \text{and} \quad \tan\phi(d_x) = \frac{\vec{x}_\nu \cdot \hat{y}}{\vec{x}_\nu \cdot \hat{x}} . \tag{2}$$

Putting this all together gives the following for the radial coordinate r, latitude θ, and longitude ϕ:

$$r = \sqrt{r_d^2 + d_x^2 + 2r_d d_x \cos\theta_\nu} , \quad \sin(\theta) = \frac{(r_d + d_x\cos\theta_\nu)\sin\theta_d + d_x \sin\theta_\nu \cos\phi_\nu \cos\theta_d}{\sqrt{r_d^2 + d_x^2 + 2r_d d_x \cos\theta_\nu}} ,$$

$$\text{and } \tan(\phi) = \frac{(r_d + d_x\cos\theta_\nu)\cos\theta_d \sin\phi_d - d_x \sin\theta_\nu (\cos\phi_\nu \sin\theta_d \sin\phi_d + \sin\phi_\nu \cos\phi_d)}{(r_d + d_x\cos\theta_\nu)\cos\theta_d \cos\phi_d - d_x \sin\theta_\nu (\cos\phi_\nu \sin\theta_d \cos\phi_d - \sin\phi_\nu \sin\phi_d)} ,$$

Case	Constant	Discontinuity	Initial θ, ϕ
$\sin\theta_\nu = 0$	θ and ϕ	$d_x = r_d$ if $\cos\theta_\nu = -1$	$-\theta_d$, $\phi_d + 180°$
$\sin\phi_\nu = 0$	ϕ	$d_x = \frac{r_d}{\cos\phi_\nu \sin\theta_\nu \tan\theta_d - \cos\theta_\nu}$	$\phi_0 = \phi_d + 180°$
$\cos\theta_d = 0$	ϕ	None	
$\sin\theta_d = 0$ and $\cos\phi_\nu = 0$	θ	None	

Table 1: Special cases noted where the latitude θ and/or longitude ϕ are constant along a neutrino's trajectory, apart from a possible jump discontinuity. The first column defines the case while the other columns specify which variable is constant, where the discontinuity is, and the value of the neutrino's latitude and longitude before reaching the discontinuity, if applicable, while going towards the detector (in all other situations, the value is the same as that of the detector).

with the signs of the numerator and denominator being used to determine the quadrant of ϕ.

Next, we carefully inverted these equations to come up with expressions for the distance from the detector in terms of each of the coordinates, paying attention to the ranges of variables over which these expressions are valid. From the place where the neutrino enters the Earth, the radial coordinate of the neutrino decreases either until it reaches the detector (for downgoing neutrinos, i.e. for $\theta_\nu \geq 0$) or until it reaches a minimum given by $r_{\min} = r_d \sin\theta_\nu$ (for upgoing neutrinos, i.e. for $\theta_\nu < 0$). Thus, the equation for d_x in terms of r is

$$d_x(r) = \begin{cases} -r_d\cos\theta_\nu + \sqrt{r^2 - r_d^2\sin^2\theta_\nu} & \text{for } d_x(r) > d_x(r_{\min}) \\ -r_d\cos\theta_\nu - \sqrt{r^2 - r_d^2\sin^2\theta_\nu} & \text{for } d_x(r) < d_x(r_{\min}) \end{cases}, \tag{3}$$

where the two cases are before and after r reaches the minimum value $d_x(r_{\min})$ on the way to the detector, and $d_x(r_{\min}) = -r_d\cos\theta_\nu$ for $\cos\theta_\nu < 0$ and 0 otherwise.

Now, moving on to the latitude and longitude, we noted several special cases that are described in table 1. We designed FillPath to take care of these cases separately as far as finding latitude and longitude bin crossings are concerned.

For all other cases, we used derivatives to characterize the behavior of the latitude and longitude along the neutrino's trajectory in order to specify domains for the inversions to be valid. For the neutrino's latitude, we found that it increases on the way to the detector when $d_x\beta > r_d\cos\phi_\nu\cos\theta_d$, where $\beta \equiv \sin\theta_\nu\sin\theta_d - \cos\theta_\nu\cos\phi_\nu\cos\theta_d$. The only thing in the above inequality that is changing along a single neutrino trajectory is d_x, which is steadily decreasing as the neutrino heads towards the detector. The resulting cases are described in table 2. If $\beta = 0$, then the neutrino's latitude is continually increasing (resp. decreasing) along its trajectory towards the detector for $\cos\phi_\nu < 0$ (resp. $\cos\phi_\nu > 0$), and the latitude equation can be easily inverted to find

$$d_x(\theta, \beta = 0) = -r_d\cos\theta_\nu\left[1 + \left(\frac{\sin\theta_\nu\sin\theta}{\sin\theta_d}\right)\left(1 - \frac{\cos^2\theta_\nu\sin^2\theta}{\sin^2\theta_d}\right)^{-1/2}\right]. \tag{4}$$

Otherwise, the inverted equation becomes

$$d_x(\theta, \beta \neq 0) = \begin{cases} \frac{r_d\cos\phi_\nu\cos\theta_d}{\sin\theta_\nu\sin\theta_d - \cos\theta_\nu\cos\phi_\nu\cos\theta_d} - \frac{r_d\sin\theta_d}{\gamma} & \text{for } \sin\theta = \pm\gamma \\ \frac{\cos\theta_\nu\sin^2\theta - \gamma\sin\theta_d + s\sin\theta_\nu\sin\theta\sqrt{\cos^2\theta - \sin^2\phi_\nu\cos^2\theta_d}}{\gamma^2 - \sin^2\theta} r_d & \text{otherwise} \end{cases}, \tag{5}$$

β	$\cos\phi_\nu$	d_x	latitude	$d_x(\theta)$	s
< 0	anything	$> \frac{r_d \cos\phi_\nu \cos\theta_d}{\beta}$	decreasing	eq. 5	+1
< 0	anything	$< \frac{r_d \cos\phi_\nu \cos\theta_d}{\beta}$	increasing	eq. 5	-1
$= 0$	< 0	anything	increasing	eq. 4	
$= 0$	> 0	anything	decreasing	eq. 4	
> 0	anything	$> \frac{r_d \cos\phi_\nu \cos\theta_d}{\beta}$	increasing	eq. 5	-1
> 0	anything	$< \frac{r_d \cos\phi_\nu \cos\theta_d}{\beta}$	decreasing	eq. 5	+1

Table 2: Scenarios for how latitude θ and distance from the detector d_x are related along a neutrino's trajectory. The first 3 columns are the conditions that define the scenario, and the last 3 columns state how the latitude changes as d_x decreases, which equation is used for $d_x(\theta)$, and what value s has in equation 5, respectively, for each scenario.

where $\gamma \equiv \sin\theta_\nu \cos\phi_\nu \cos\theta_d + \cos\theta_\nu \sin\theta_d$ and $s = \pm 1$ with the sign being determined from table 2. It may appear that it could be possible for either of the denominators in the $\sin\theta = \pm\gamma$ case of equation 5 to be 0, but in fact, that will not happen outside of the previously addressed scenarios.

For the neutrino's longitude, we found that it is continually increasing (decreasing) along its trajectory on its way to the detector if $\sin\phi_\nu > 0$ ($\sin\phi_\nu < 0$). Thus, the longitude equation can be easily inverted to find

$$d_x(\phi) = \frac{\cos\theta_d \,(\tan\phi_d - \tan\phi)\, r_d}{(\tan\phi_d - \tan\phi)\,\alpha + \sin\theta_\nu \sin\phi_\nu \,(1 + \tan\phi_d \tan\phi)}\,, \tag{6}$$

where $\alpha \equiv \sin\theta_\nu \cos\phi_\nu \sin\theta_d - \cos\theta_\nu \cos\theta_d$.

Finally, we used these expressions in FillPath to find at which values of the distance from the detector the neutrino changes latitude, longitude, and radial bins.

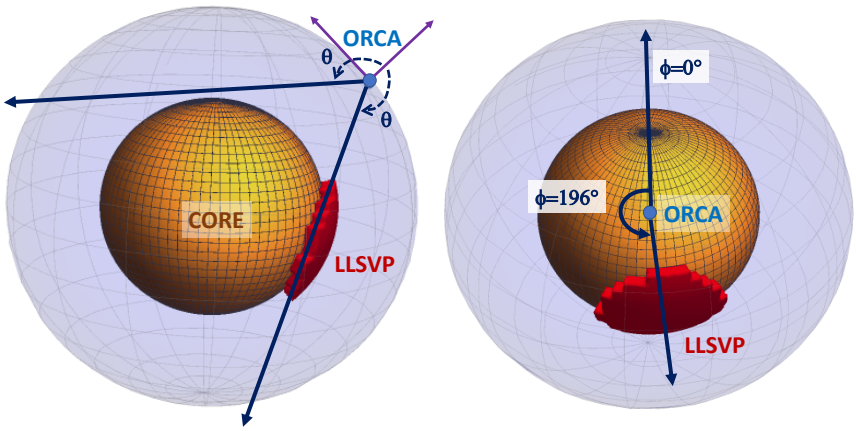

Figure 3: Two different views of the shape and location of the LLSVP (red) in the 3D Earth model used for validation purposes. The Earth's core is shown in yellow, with the edges of the latitude and longitude bins on the core's surface shown in black, and the location of the ORCA detector is shown as a blue point, with example neutrino trajectories with the same zenith and different azimuths ($\phi = 0°$ and 196°).

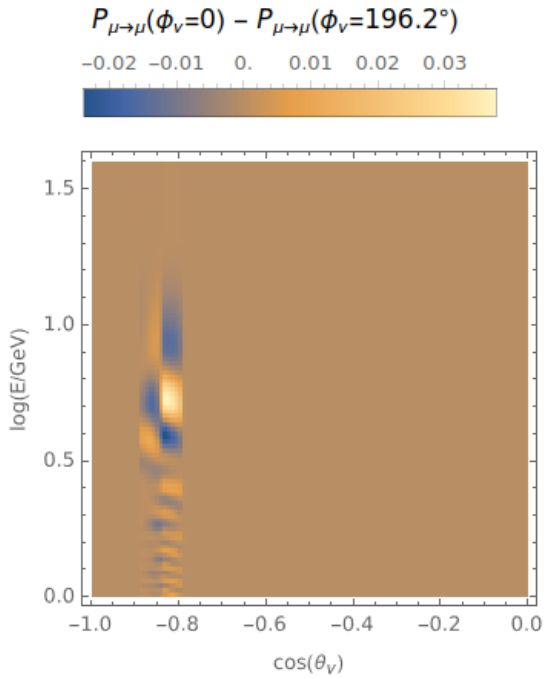

Figure 4: Difference in muon neutrino disappearance probabilities between $\phi_\nu = 0$ and $\phi_\nu = 196.2°$ (which goes through the middle of the LLSVP) as a function of the neutrino energy and zenith angle, when considering a LLSVP with 3% overdensity wrt PREM.

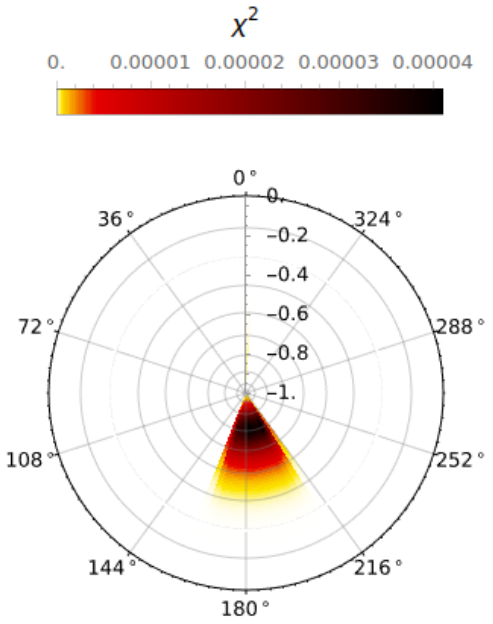

Figure 5: χ^2 plot on a polar ϕ_ν vs $\cos\theta_\nu$ plane, comparing, without marginalization, the expected events in each energy bin with the LLSVP to those without the LLSVP. Smearing is done over the neutrino's energy and zenith angle θ_ν, but not over its azimuthal angle ϕ_ν.

4. Outlook

For validation purposes, we created a binned 3D Earth model that was identical to the default PremModel, except for having a region that mimics a simplified version of the African LLSVP, in the form of a pancake with 3600 km diameter and 440 km thickness, as shown in figure 3. The chosen binning of the Earth had 42 radial bins, 36 latitude bins, and 72 longitude bins. For two scenarios of the LLSVP's density (same as PREM and 3% larger than PREM) and a detector at the location of the KM3NeT/ORCA neutrino telescope [16], we used OscProb to calculate the oscillation probabilities for 100 values each of the neutrino's energy, zenith angle θ_ν, and azimuthal angle ϕ_ν. A sample of the differences in oscillation probabilities obtained with/without LLSVP overdensity is shown in figure 4.

Based on the oscillation probabilities calculated with OscProb, we then computed the expected number of events in an ORCA-like detector for both scenarios, using the EarthProbe framework described in [12], augmented to include the azimuthal angle dependance (assuming perfect detector resolution for that angle so far). We calculated bin-by-bin $\Delta\chi^2$ values for track and shower events separately, when fitting the events for the LLSVP overdensity with the events for the case with no LLSVP, without including minimization over any of the model parameters. As can be seen from figure 5, the "shadow" of an overdense LLSVP indeed appears in the resulting $\Delta\chi^2$ angular distribution, after summing over the neutrino energy bins and including both event topologies

detected by ORCA. Once the framework is extended to account for detector effects related to azimutal resolution, we expect that it provides a comprehensive tool for studying the potential of present and future neutrino detectors to investigate LLSVPs and other inhomogeneities in the Earth's interior.

Acknowledgements

The authors acknowledge financial support of the LabEx UnivEarthS at Université Paris Cité (ANR-10-LABX-0023 and ANR-18-IDEX-0001)

References

[1] von Rebeur-Paschwitz, E., The earthquake of Tokio, April 18, 1889, Nature, 40 294-295, 1889.

[2] Dziewonski, A. M., and Anderson, D. L., Preliminary reference Earth model, Physics of the Earth and Planetary Interiors, Volume 25, Issue 4, Pages 297-356 (1981), https://doi.org/10.1016/0031-9201(81)90046-7.

[3] Dziewonski, A., B. Hager, and R. O'Connell, Large-scale heterogeneities in the lower mantle, J. Geophys. Res., 82, 239–255 (1977).

[4] French, S.W., and Romanowicz, B., Broad plumes rooted at the base of the Earth's mantle beneath major hotspots, Nature, 525, 95-99 (2015).

[5] S. Durand, E. Debayle, Y. Ricard, and S. Lambotte, Seismic evidence for a change in the large-scale tomographic pattern across the D" layer, Geophys. Res. Lett. 43 (15), 7928–7936 (2016).

[6] Garnero.J., and McNamara, A. K., Structure and dynamics of Earth's lower mantle. Science 320(5876):626-8 (2008) doi: 10.1126/science.1148028. PMID: 18451293.

[7] Labrosse, S., J. W. Hernlund, and N. Coltice, A crystallizing dense magma ocean at the base of the Earth's mantle, Nature, 450(7171), 866– 869 (2007).

[8] Garnero, J.E., McNamara, A.K., Shim, S.-H., Continent-sized anomalous zones with low seismic velocity at the base of Earth's mantle, Nature geoscience, doi: 10.1038/ngeo2733 (2016).

[9] McNamara, A. K. review of large low shear velocity provinces and ultra low velocity zones, Tectonophysics, 760, 199-220 (2019).

[10] Rott, C., Taketa, A., and Bose, D., Spectrometry of the earth using neutrino oscillations. Sci. Rep. 5, 15225, 2015. doi:10.1038/srep15225

[11] Winter, W., Atmospheric neutrino oscillations for earth tomography. Nucl. Phys. B908, 250–267 (2016). doi:10.1016/j.nuclphysb.2016.03.033

[12] L. Maderer *et al.*, Front. Earth Sci., 14 (2023) Sec. Solid Earth Geophysics Vol. 11 - https://doi.org/10.3389

[13] Coelho, J. A. B., et al. (2023). joaoabcoelho/OscProb (v.1.6.1). Zenodo. https://doi.org/10.5281/zenodo.8074017.

[14] Brun R., et al. (2019). root-project/root (v6-18-02). Zenodo. https://doi.org/10.5281/zenodo.3895860.

[15] https://earthref.org/GERMRD/datamodel/; McDonough, W.F. (2004). Compositional Model for the Earth's Core. In: Treatise on Geochemistry. Holland, H.D. and Turrekian, K.K. (Editors), Elsevier, Amsterdam, The Netherlands. 2: 547-568; Wedepohl, K.H. (1995). The composition of the continental crust. Geochimica et Cosmochimica Acta 59: 1,217-1,239. doi: 10.1016/0016-7037(95)00038-2; Quinby-Hunt, M.S. and Turekian, K.K. (1983). Distribution of elements in sea water. EOS, Transactions of the American Geophysical Union 64: 130-132; Prinn, R.G. (2004). Ozone, Hydroxyl Radical, and Oxidative Capacity. In: Treatise on Geochemistry. Holland, H.D. and Turekian, K.K. (Editors), Elsevier, Amsterdam. 4: 1-19.

[16] S. Adrian-Martinez et al. [KM3NeT Coll.], Letter of intent for KM3NeT 2.0, J. Phys. G43(8), 084001 (2016).